Ann. Phys. (Berlin) 524, No. 6–7, 327–337 (2012) / DOI 10.1002/andp.201200055

annalen der physik

Quantum disc plus inverse square potential. An analytical model for two-dimensional quantum rings: Study of nonlinear optical properties

Carlos M. Duque[1], *Miguel E. Mora-Ramos*[2,*], *and Carlos A. Duque*[1]

Received 15 March 2012, revised 19 April 2012, accepted 3 May 2012
Published online 22 May 2012

The exact solutions for the two-dimensional motion of a conduction band electron in a disc shaped quantum dot under the effect of an external magnetic field and parabolic and inverse square confining potentials are used to calculate the linear and nonlinear optical absorption as well as the linear and nonlinear corrections to the refractive index in the system. It is shown that this kind of structure may work well as a model for a quantum ring. Using the basic parameters typical of the GaAs, the results show that the influence of the normally oriented magnetic field induces a blueshift in both the first and third order peaks of the calculated optical quantities. In addition, total peak amplitudes are shown to be growing functions of the magnetic field strength. The increase in the strength of the inverse square potential function enhances significantly the contribution from the nonlinear third-order terms in both the absorption and the relative correction to the refractive index.

1 Introduction

The description of the parabolic – and semi-parabolic – confinement of charge carriers in quantum nanostructures has been put forward in a rather large number of reports in the last two decades. To mention just a few, we may refer here to earlier works dealing with the study of optical properties [1–3], and hydrogenic impurity binding energies [4] in quantum wells. Moreover, one may find more recent studies dealing with the particular features of the optical properties in this kind of parabolically confined systems [5–7].

The use of self-assembly techniques has made possible the fabrication of quantum dot (QD) and quantum ring (QR) semiconductor structures by using the so-called self-assembly techniques (see, for instance, the reference [8]). Both QD and QR systems are a subject of great interest due to their prospective applications in the design and production of optoelectronic devices [9–12]. On the other hand, if the subject goes beyond the case of single nanostructures, the artificial molecules consisting of coupled QDs or QRs are particularly attractive because they show great promise for quantum information processing [13] and terahertz device production [14].

By extending the semiclassical theory of Balian and Bloch, Tatievski et al. [15] have determined the electronic shell structure resulting from the interference of closed orbital paths for mesoscopic systems like spherical clusters, discs and rings. They have obtained analytical results for the shell structure in the density of states, an useful tool to calculate oscillations in the binding-energy and ionization potentials. Tan and Inkson [16] have used an exactly soluble model to study magnetization and persistent currents of electrons confined in two-dimensional mesoscopic rings and dots which allows the calculation of magnetization and persistent currents for a range of device geometries containing a large number of electrons. They showed that in the weak-magnetic-field limit, the persistent current is simply proportional to the magnetization, presenting Aharonov-Bohm type oscillations. In the same direction, the investigation of equilibrium electron currents and magnetization in an ideal two-dimensional disk under the presence of a strong magnetic field has been carry out by Avishai and Kohmoto [17].

* Corresponding author E-mail: memora@uaem.mx
[1] Instituto de Física, Universidad de Antioquia, AA 1226, Medellín, Colombia
[2] Facultad de Ciencias. Universidad Autónoma del Estado de Morelos. Ave. Universidad 1001. CP. 62209. Cuernavaca. Morelos. México

The investigation of linear and nonlinear optical response in parabolic QDs has also given rise to a number of reports, among which we can mention those in references [18, 19]. In addition, there is a particular type of quasi-zero-dimensional system known as quantum disc (QDC) – or disc-shaped quantum dot – , which has also attracted some attention [20–22]. That is precisely the type of system we are dealing with in the present work.

This article is devoted to the study of the electronic states in quantum discs under the combined influence of two distinct confining profiles: a parabolic-type, and the one provided by a potential energy function with inverse square dependence. All this is complemented with the presence of an externally applied magnetic field. The inverse square potential function appeared as a model for the inter-particle interaction in the study of the quantum problem of N particles in a two-dimensional parabolic potential under a magnetic field [23]. We discuss here that its inclusion, together with the other two potential fields, might lead to a rather direct modeling for the states of carriers confined in a two-dimensional semiconducting QR. It will be shown that the single electron eigenstates of the corresponding Schrödinger-like conduction band effective mass equation can be exactly described via analytical expressions in this case. Then, we shall apply the obtained energy levels and wavefunctions in order to calculate the linear and nonlinear optical absorption and relative refractive index variation in a GaAs-based system bearing such a geometry. The paper is organized as follows. In Sect. 2 we describe the theoretical framework. Section 3 is dedicated to the discussion of the obtained results, and our conclusions are given in Sect. 4.

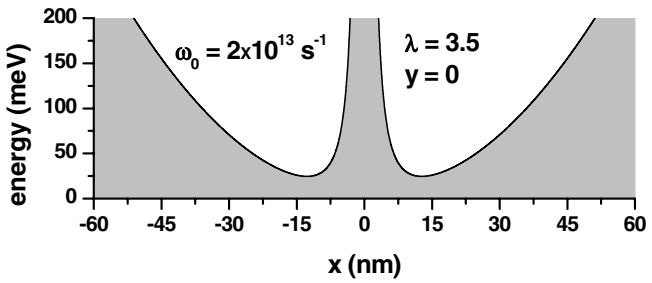

Figure 1 A cross-view showing the potential energy profile along the direction $\varphi = 0$.

2 Theoretical framework

Consider the motion of a confined electron in a disc shaped quantum dot (DSQD). Then, the polar system (r, φ) is a suitable set of coordinates for the description of the allowed quantum states. Taking into account the presence of a static magnetic field **B**, oriented along the positive normal to the plane (here named as z-direction), the Hamiltonian of the system, within the framework of the effective mass approximation, is given by

$$H = \frac{1}{2m^*}\left[\mathbf{p} + \frac{q}{c}\mathbf{A}\right]^2 + V(\mathbf{r}), \tag{1}$$

where q, m^* and c are the absolute value of the electron charge, the electron effective mass, and speed of light respectively. $\mathbf{A} = (A_r = 0, A_\varphi = \frac{Br}{2}, A_z = 0)$ is the vector potential of the static magnetic field. We are assuming here the presence of a confining potential, $V(\mathbf{r})$, which combines a parabolic and inverse squared potential functions;

$$V(\mathbf{r}) = \frac{1}{2}m^*\omega_0^2 r^2 + \frac{\hbar^2}{2m^*}\frac{\lambda}{r^2}, \tag{2}$$

where ω_0 represents the confinement frequency and the dimensionless parameter λ characterizes the strength of the the external field, with $\lambda < 0$ describing an attractive potential and $\lambda \geq 0$ a repulsive one. In the present work, we take $\lambda \geq 0$ which enables us to calculate solutions for the lower energy bound since the attractive potential has no lower energy bound.

Now, if use the Coulomb gauge ($\nabla.\mathbf{A} = 0$), and use the fact that $\nabla.(\mathbf{A}\psi) = \mathbf{A}.(\nabla\psi) + (\nabla.\mathbf{A})\psi = \mathbf{A}.(\nabla\psi)$ the Schrödinger equation in polar coordinates has the form

$$\left[-\frac{\hbar^2}{2m^*}\left(\frac{\partial^2}{\partial r^2} + \frac{1}{r}\frac{\partial}{\partial r} + \frac{1}{r^2}\frac{\partial^2}{\partial\varphi^2}\right) + \frac{1}{2}m^*\Omega^2 r^2 + \frac{\hbar^2}{2m^*}\frac{\lambda}{r^2} + \frac{\omega_c}{2}L_z\right]\psi = E\psi, \tag{3}$$

where $\omega_c = \frac{qB}{m^*c}$ is known as the cyclotron frequency, $\Omega = \sqrt{\omega_0^2 + \frac{\omega_c^2}{4}}$ is the total confinement frequency in the magnetic field, E is the energy eigenvalue, and L_z is the orbital angular momentum operator along the z-direction, respectively. To find the solution of (3) that corresponds to a two-dimensional eigenstate ψ, it is customary to propose

$$\psi(r,\varphi) = \frac{\chi(r)}{\sqrt{r}}\frac{e^{im\varphi}}{\sqrt{2\pi}}, \tag{4}$$

where m is an integer usually named as magnetic quantum number. The combination of (3) and (4) allows to obtain an equation for $\chi(r)$ in the form

$$\frac{d^2\chi}{dr^2} + \left[\frac{2m^*\mathscr{E}}{\hbar^2} - \frac{m^*\Omega^2}{\hbar^2}r^2 - \frac{m^2 + \lambda - 1/4}{r^2}\right]\chi = 0, \tag{5}$$

with

$$\mathscr{E} = E - \frac{m\hbar\omega_c}{2}. \tag{6}$$

Now, we may perform two more typical changes: $l(l+1) = m^2 + \lambda - 1/4$ and $\rho = r^2$. With this, it is possible to rewrite the differential equation (5) as follows;

$$\frac{d^2\chi}{d\rho^2} + \frac{1}{2\rho}\frac{d\chi}{d\rho} - \left[\frac{1}{4} + \frac{l(l+1)}{4\rho^2} - \frac{m^*\mathscr{E}}{2\hbar^2\rho}\right]\chi = 0, \tag{7}$$

where the only solution of the quadratic equation for l with physical meaning is:

$$l = -\frac{1}{2} + \sqrt{\lambda + m^2}. \tag{8}$$

Defining

$$\eta = \sqrt{\frac{\hbar}{m^*\Omega}}, \quad \kappa = \frac{\mathscr{E}}{2\hbar\Omega}, \quad s_m = \frac{l+1}{2} = \frac{1}{4} + \frac{\sqrt{\lambda + m^2}}{2}$$

and setting $\rho = \eta^2 z$, Eq. (7) can be written as

$$\frac{d^2\chi}{dz^2} + \frac{1}{2z}\frac{d\chi}{dz} - \left[\frac{1}{4} + \frac{s_m(s_m - 1/2)}{z^2} - \frac{\kappa}{z}\right]\chi = 0. \tag{9}$$

Taking into account the asymptotic behavior at the origin and at the infinity for the wave function, we can propose the following ansatz for the well-defined solutions at those two limits:

$$\chi(z) = z^{s_m} e^{-z/2} F(z), \tag{10}$$

leading us to the equation

$$z\frac{d^2F}{dz^2} + (b - z)\frac{dF}{dz} - aF = 0, \tag{11}$$

known as Kummer's differential equation, whose solution is the confluent hypergeometric function [25]. Here $b = 2s_m + 1/2$ and $a = s_m + 1/4 - \kappa$. The solutions of this equation that guarantee that $\chi(z)$ remains finite require the parameter a to become a negative integer, $-n$. In this case, the confluent hypergeometric function reduces to a polynomial of n-th degree. Here, we are going to use the representation

$$F(-n, b; x) = \frac{\Gamma(1+n)\Gamma(b)}{\Gamma(b+n)} L_n^{b-1}(x), \tag{12}$$

where $\Gamma(c)$ is the Euler gamma function, and $L_n^{b-1}(x)$ are the so-called associated Laguerre polynomials.

With the aid of (4) and (10) we can write

$$\psi(r,\varphi)_{mn} = \frac{N_{mn}}{\sqrt{r}} r^{2s_m} e^{-r^2/2\eta^2} L_n^{2s_m - 1/2}(r^2/\eta^2) e^{im\varphi}, \tag{13}$$

where the normalization constant is determined by means of the orthonormality condition

$$\int_0^\infty x^\alpha e^{-x} L_n^\alpha(x) L_m^\alpha(x) dx = \frac{\Gamma(n+\alpha+1)}{n!}\delta_{nm} \tag{14}$$

as

$$N_{mn} = \sqrt{\frac{n!}{\pi\Gamma(2s_m + n + 1/2)\eta^{4s_m+1}}}. \tag{15}$$

By using $n = \frac{\mathscr{E}}{4\hbar\Omega} - s_m - \frac{1}{4}$ and $\mathscr{E} = E - \frac{m\hbar\omega_c}{2}$, we can obtain the energy spectrum of the confined states as

$$E_{mn} = (2n + 1 + \sqrt{\lambda + m^2})\hbar\sqrt{\omega_0^2 + \frac{\omega_c^2}{4}} + \frac{m\hbar\omega_c}{2} \tag{16}$$

As it can be seen from the Fig. 1, if $\lambda \neq 0$, there will be a spatial region in the disc shaped quantum dot in which the repulsive potential barrier centered at the origin is significantly high, and strong enough to keep the electrons far from reaching values of the radial component close to $r = 0$. This means that the behavior of the carrier system will largely resemble that of the electrons

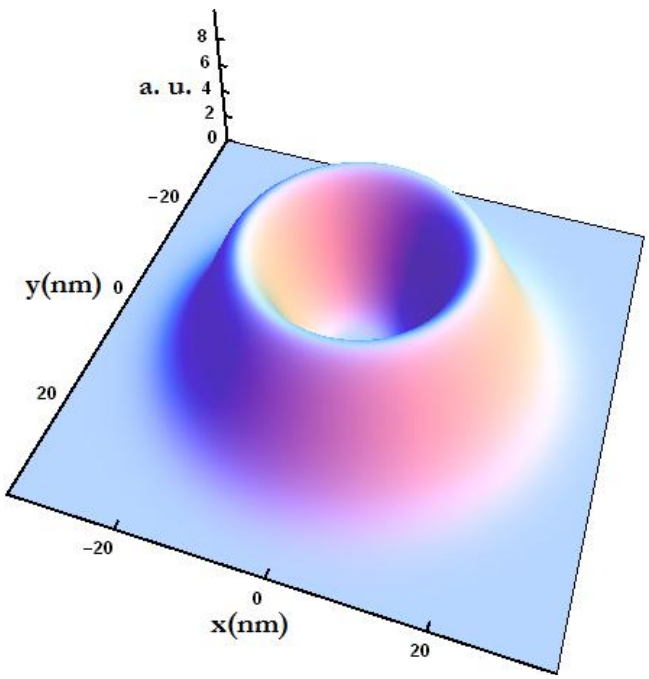

Figure 2 (online color at: www.ann-phys.org) The probability density corresponding to the ground state wave function obtained from Eqs. (13), (15), and (16). The values of ω_0 and λ are the same used in the Fig. 1.

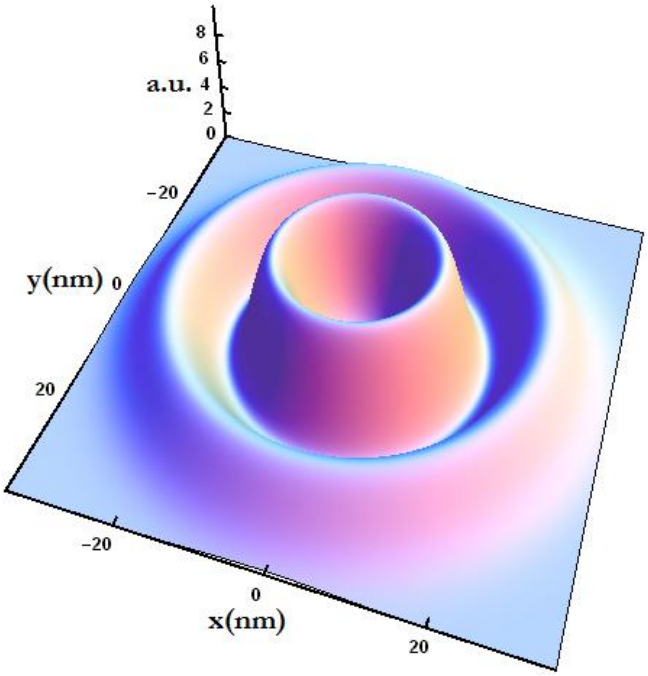

Figure 3 (online color at: www.ann-phys.org) The same as in Fig. 2, but for the case of the wave function that corresponds to the first excited electron state.

confined in a quantum ring. This is confirmed by observing the Figs. 2 and 3, where we are depicting the probability density corresponding to the ground and first excited electron states in the system under study. There, the shape of $|\psi|^2$ indicates that the radial region around the origin is forbidden for the carriers given the repulsive effect of the inverse square barrier. Then, the use of the present model, with a suitable combination of both ω_0 and λ could be useful for the simulation of actual quantum rings, provided the advantages of having analytical expressions for both the wave functions and eigenvalues of the problem.

Among the many applications that these states may have, we choose in this work to apply them in the calculation of linear and nonlinear optical coefficients in DSQD (or – as commented above – parabolic 2D QR) provided this kind of systems are attracting much interest in optoelectronics. Given that some intersubband energy intervals, together with their corresponding dipole matrix elements, will be used to calculate the absorption coefficients, we will choose here the energy levels and the wave functions participating in the transition as

$$E_1 = E_{00}, \quad E_2 = E_{11}, \quad \psi_1 = \psi_{00}, \quad \psi_2 = \psi_{11}, \tag{17}$$

hence, the energy difference E_{21} between E_2 and E_1, is expressed as:

$$E_{21} = (2 + \frac{1}{\sqrt{\lambda+1}+\sqrt{\lambda}})\hbar\sqrt{\omega_0^2 + \frac{\omega_c^2}{4}} + \frac{\hbar\omega_c}{2}. \tag{18}$$

Finally, the electric dipole transition matrix elements are written as

$$M_{21} = \left|q\left\langle\psi_2\left|r\cos\varphi\right|\psi_1\right\rangle\right|$$
$$= \frac{q\pi}{2}N_{00}N_{11}\lambda^{2(s_0+s_1+1)}\frac{(s_1-s_0-1/2)!}{(s_1-s_0-3/2)!}\Gamma(s_0+s_1+1), \tag{19}$$

and taking into account the electric dipole selection rules we have

$$M_{22} = M_{11} = 0. \tag{20}$$

We shall also give in this section a brief derivation of the linear and third-order nonlinear optical absorption coefficient due to intersubband transitions in a DSQD by the compact density matrix method and the iterative procedure. The approach assumes the interaction of polarized monochromatic electromagnetic radiation with the DSQD. The electric field of this optical wave is

$$E(t) = E_0\cos(\omega t) = \tilde{E}\exp(-i\omega t) + \tilde{E}\exp(i\omega t). \tag{21}$$

Let us denote ρ as the one-electron density matrix for the system. Then the evolution of the density matrix operator ρ obeys the following time-dependent equation

$$\frac{\partial\rho_{ij}}{\partial t} = \frac{1}{i\hbar}[H_0 - qxE(t), \rho]_{ij} - \Gamma_{ij}(\rho - \rho^0)_{ij}, \tag{22}$$

where H_0 is the Hamiltonian of the system in the absence of the electromagnetic field $\tilde{E}(t)$, $\rho^{(0)}$ is the unperturbed density matrix, and Γ_{ij} is the phenomenological relaxation rate, caused by the electron-phonon, electron-electron and other collision processes. Here we select $\Gamma_{ij} = \Gamma_0 = 1/T_0$ when $i \neq j$ for simplicity.
It is possible to solve (22) by using an iterative method that incorporates the different orders of the dielectric susceptibility response to the electric field wave. This implies proposing a solution in the form

$$\rho(t) = \sum_n \rho^{(n)}(t), \tag{23}$$

which, after substitution in Eq. (22) allows to write the following set of relations between the n-th and $(n+1)$-th order terms [24]:

$$\frac{\partial\rho_{ij}^{(n+1)}}{\partial t} \tag{24}$$
$$= \frac{1}{i\hbar}\{[H_0, \rho^{(n+1)}]_{ij} - i\hbar\Gamma_{ij}\rho_{ij}^{(n+1)}\} - \frac{1}{i\hbar}[qx, \rho^{(n)}]_{ij}E(t).$$

Considering terms up to third order in the electronic polarization of the DSDQ, due to the electric field, we can write

$$P(t) = \epsilon_0 \chi_\omega^{(1)} \tilde{E} e^{i\omega t} + \epsilon_0 \chi_\omega^{(3)} \tilde{E} e^{3i\omega t} + c.c, \tag{25}$$

where ϵ_0 is the vacuum permittivity, $\chi_\omega^{(1)}$ and $\chi_\omega^{(3)}$ are the linear and third-order nonlinear susceptibility coefficients, respectively. The electronic polarization of the n-th order electronic polarization is given as

$$P^{(n)}(t) = \frac{1}{V} Tr(\rho^{(n)} qx), \tag{26}$$

where V is the volume of interaction and Tr denotes the trace or summation over the diagonal elements of the matrix $\rho^{(n)} ex$.

After taking into account (20), the expressions for the linear and third-order nonlinear optical absorption coefficients are, respectively,

$$\alpha^{(1)}(\omega) = \omega \sqrt{\frac{\mu}{\epsilon_R}} \frac{|M_{21}|^2 \sigma_v \hbar \Gamma_0}{(E_{21} - \hbar\omega)^2 + (\hbar\Gamma_0)^2} \tag{27}$$

and

$$\alpha^{(3)}(\omega) = -\sqrt{\frac{\mu}{\epsilon_R}} \left(\frac{4I\omega}{2\epsilon_0 n_r c}\right) \frac{|M_{21}|^4 \sigma_v \hbar \Gamma_0}{\left[(E_{21} - \hbar\omega)^2 + (\hbar\Gamma_0)^2\right]^2}, \tag{28}$$

where σ_v is the electron density of the DSQD, μ is the permeability of the system, $\epsilon_R = \epsilon_0 n_r^2$ (n_r is the refractive index) is the real part of the permittivity, $\hbar\omega$ is the incident photon energy, and $I = 2\epsilon_0 n_r c |\tilde{E}|^2$ is the incident optical intensity. Therefore, the total optical absorption coefficients can be written as

$$\alpha(\omega) = \alpha^{(1)}(\omega) + \alpha^{(3)}(\omega). \tag{29}$$

In a similar manner it is possible to obtain the linear and third-order nonlinear relative refractive index change whose expressions are, respectively,

$$\frac{\triangle n^{(1)}(\omega)}{n} = \frac{\sigma_v |M_{21}|^2}{2n^2 \epsilon_0} \frac{E_{21} - \hbar\omega}{(E_{21} - \hbar\omega)^2 + (\hbar\Gamma_0)^2} \tag{30}$$

and

$$\frac{\triangle n^{(3)}(\omega)}{n} = -\frac{\sigma_v \mu c I |M_{21}|^4}{n^3 \epsilon_0} \frac{E_{21} - \hbar\omega}{\left[(E_{21} - \hbar\omega)^2 + (\hbar\Gamma_0)^2\right]^2}, \tag{31}$$

where (20) was again taken into account. Finally the total relative refractive index change can be calculated as

$$\frac{\triangle n(\omega)}{n} = \frac{\triangle n^{(1)}(\omega)}{n} + \frac{\triangle n^{(3)}(\omega)}{n}. \tag{32}$$

3 Results and discussion

In this section we present our calculations for the optical absorption and refractive index change in the type of 2D-quantum dot under study. The prototypical system considered consists of a GaAs-based DSQD, and the values of the confining potential input parameters are those reported in the caption linked to Fig. 4. Moreover, the different constants appearing in the expressions above are: $\sigma_v = 5 \times 10^{22}\,\mathrm{m}^{-3}$, $\Gamma_0 = 1/(0.14\,\mathrm{ps})$, $c = 3 \times 10^8\,\mathrm{m/s}$ (the speed of light in vacuum), $\epsilon_0 = 8.85 \times 10^{-12}\,\mathrm{F/m}$, $\mu = 1.256, \times 10^{-6}\,\mathrm{T\,m/A}$, $n_r = 3.2$, $q = 1.6 \times 10^{-19}\,\mathrm{C}$, and $m^* = 0.067\,m_0$, where m_0 is the free electron mass.

In the Fig. 4(a) one can observe the behavior of the linear, third-order nonlinear and total optical absorption coefficients, calculated as functions of the photon energy. Several distinct values of the applied static magnetic field have been taken into account, as it may be seen from the different curves presented. From the results depicted it is possible to conclude that, as it should be expected, the the main contributions come from the linear term since the third-order coefficient just induces a comparatively small contribution. There is a resonant peak located in $\hbar\omega = E_{21}$ which suffers a blueshift as there is a raising in the magnetic field intensity. By considering the expression (16) for the energy levels, one sees that E_{21} directly depends on ω_c; that is, with the field amplitude, B. Therefore, when there is an increase of the field intensity, the effect is to move the resonant energy towards higher energy values.

On the other hand, in the Fig. 4(b) we notice the variation of the maximum peak intensity of the coefficients as a function of the magnetic field. Here, the combination of two main reasons can explain the variation in the peak intensities: On one side, we have the variation associated to changes in the value of the electric dipole matrix element $|M_{21}|$. This quantity tends to decrease with the the magnetic field intensity until it reaches an asymptotic value, in which case it is not possible to keep a progressive confining of the electron in the system. In such a way, the wave functions of the system stop varying which leads to a constant value of $|M_{21}|$. On the other side, we realize that the peak intensities vary as a result of the magnetic field provided that the coefficients are proportional to the frequency of resonance, E_{21}, and this quantity grows linearly for sufficiently high magnetic field strengths, as can be deduced from the Eq. (18). Such energy difference does not have an upper limit value, therefore we may characterize it as the most influent factor in the behavior of the peak intensities. This is true because it affects mainly the dependence of the linear optical absorption coefficient, which dominates in the overall re-

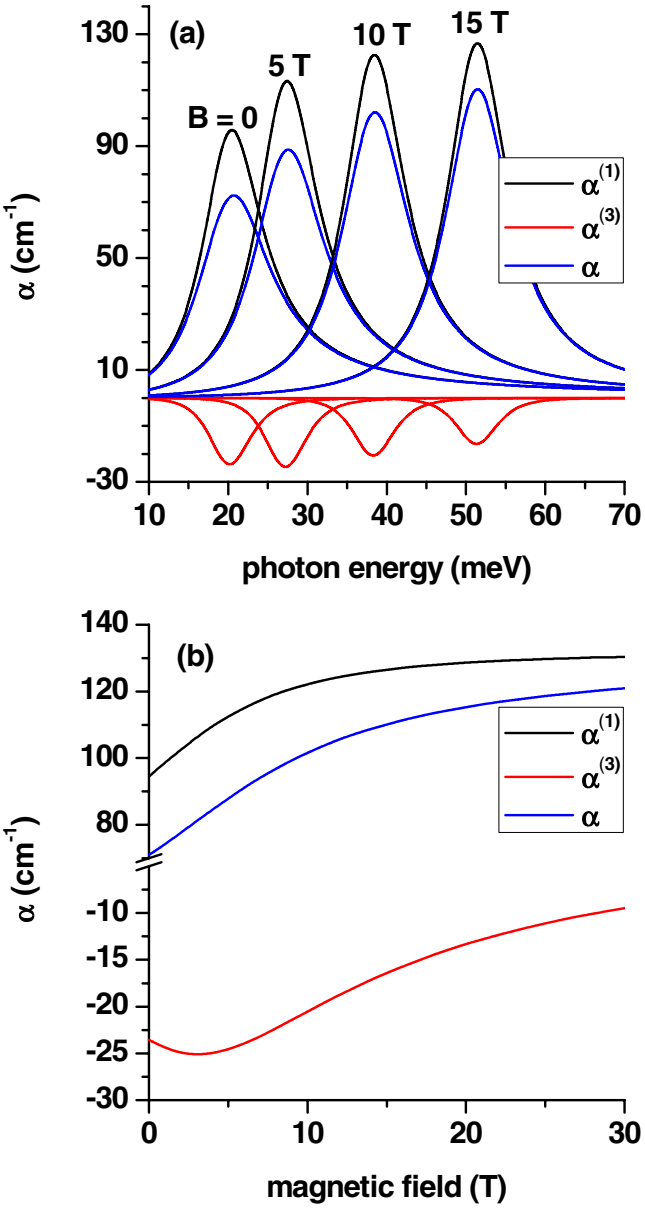

Figure 4 (online color at: www.ann-phys.org) Linear (black line), third-order nonlinear (red line) and total (blue line) optical absorption coefficients as a function of the photon energy (a) and magnetic field (b) with $\omega_0 = 1.2 \times 10^{13}\,\mathrm{s}^{-1}$, $\lambda = 0.5$, and $I = 1.5 \times 10^{10}\,\mathrm{W/m}^2$ for Fig. (a). In Fig. (b) we use the same parameters as well as $\hbar\omega = E_{21}$.

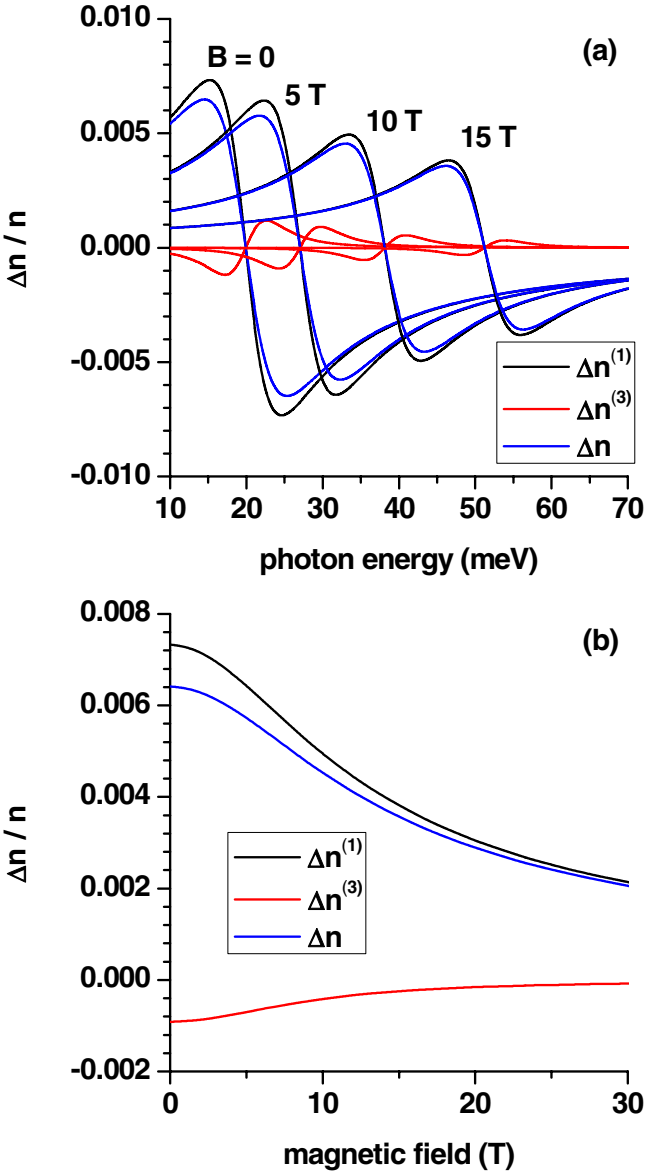

Figure 5 (online color at: www.ann-phys.org) Linear (black line), third-order nonlinear (red line) and total (blue line) relative refractive index change as a function of the photon energy (a) and magnetic field (b) with $\omega_0 = 1.2 \times 10^{13}\,\mathrm{s}^{-1}$, $\lambda = 0.5$, and $I = 1.5 \times 10^{10}\,\mathrm{W/m}^2$ for Fig. (a). In Fig. (b) we use the same parameters as well as $\hbar\omega = E_{21} - \hbar\Gamma_0$.

sult. The third-order coefficient contributes more significantly in the region of small field intensities, in which the increase of the energy difference E_{21} is the main factor in the variation. Then, for larger field strength, the decreasing tendency of the dipole matrix elements becomes the leading effect in the monotony of the nonlinear optical absorption coefficient. It is possible to see that the first and total coefficients tend to have the same behavior but it is more visible as we reach sufficiently high magnetic fields due to the fact that at such large values of B, the contribution of $\alpha^{(3)}$ is practically negligible.

The outcome of an analogous calculation but for the relative change in the refractive index is the one presented in the Fig. 5. Figure 5(a) contains the linear and third-order nonlinear contributions as well as total relative change, all depicted as functions of the incident photon energy. Again, a set of different values of the magnetic field strength are used as input parameters. According to the discussion made above, augmenting the field intensity leads to a blueshift in the positions of the peaks since, as can be seen from Eqs. (30) and (31), these quantities are directly related with the difference $E_{21} - \hbar\omega$. Also, one readily observes that, contrary to the case of the optical absorption coefficients, the growth in the magnitude of B has the consequence of a reduction in the $\Delta n/n$ peak amplitudes. Looking once again at the same two equations we realize that the variation responsible for such a dependence is that of $|M_{21}|$ vs $\hbar\omega = E_{21}$. Now, there is no factor proportional to ω that can influence on the value of the coefficients. Therefore, the monotonous evolution of the dipole matrix elements towards a smaller limiting value for high enough field strengths dictates the observed behavior. One may readily notice that by observing the Fig. 5(b). There, the magnitude of the linear, nonlinear and total resonant peak amplitudes are shown as decreasing functions of B; thus confirming the above made discussion.

The Fig. 6(a) shows our results for the linear, third-order nonlinear and total optical absorption coefficients as functions of the photon energy. In this case we keep the magnetic field to remain constant, and vary the dimensionless parameter λ. As a consequence of this, there is observed a non perceptible redshift of the resonant peak but the sizes of the peaks do present significant variations. At a first glance, it is possible to see that when λ increases its value, not only the first-order peak increases its size but also the third-order peak does it. This behavior allows us to conclude that when the inverse square potential parameter acquires sufficiently large values, the confinement potential is strong enough as to prevent us from neglecting the contribution of the third order coefficient – even if the first order contribution is significantly stronger. The variation of the peak intensities can be explained on the basis of the arguments presented in the comments about Fig. 4. But this time we must clarify that the matrix element $|M_{21}|$ tends to grow as we increase λ, whereas the energy difference E_{21} decreases with λ given that it has an inverse dependence on it. However, it should be stressed that, in this situation, the role of dominant quantity is represented by $|M_{21}|$; which explains why also in this case, the peaks tend to increase their intensities with larger values of λ. From Fig. 6(b) we can corroborate our previous arguments since one may see that

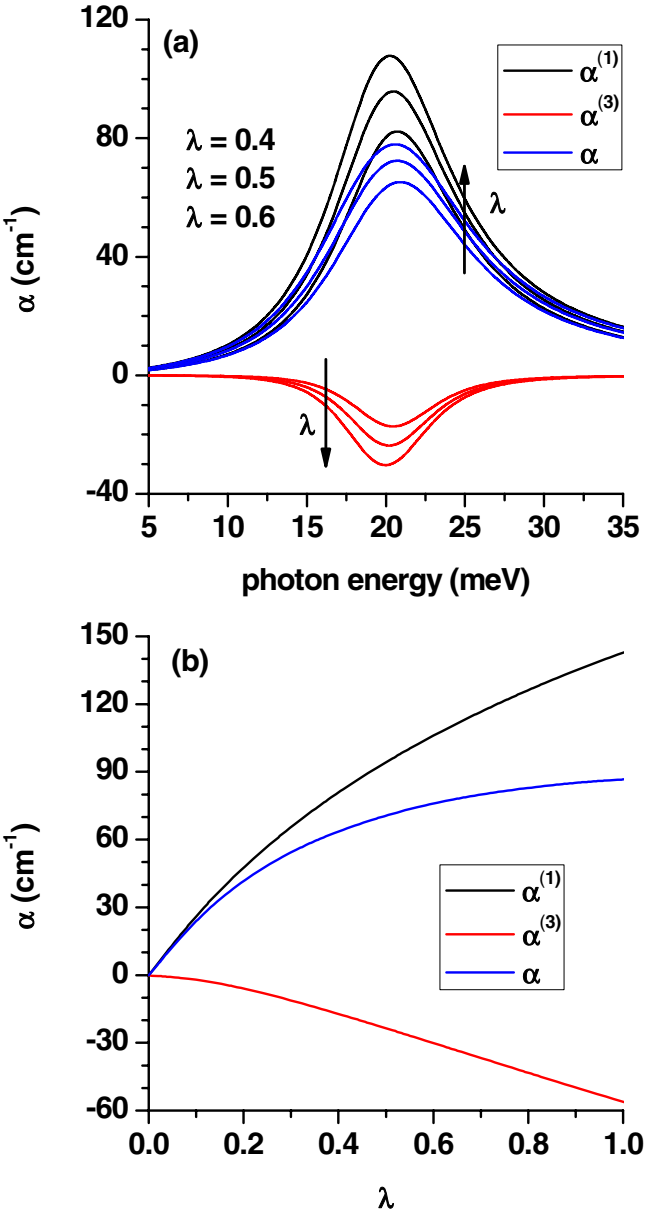

Figure 6 (online color at: www.ann-phys.org) Linear (black line), third-order nonlinear (red line) and total (blue line) optical absorption coefficients as a function of the photon energy (a) and the dimensionless parameter λ (b) with $\omega_0 = 1.2 \times 10^{13}\,\mathrm{s}^{-1}$, $B = 0$, and $I = 1.5 \times 10^{10}\,\mathrm{W/m}^2$ for Fig. (a). The direction of the arrows determines in which direction is raising λ for the optical absorption coefficients. In Fig. (b) we use the same parameters as well as $\hbar\omega = E_{21}$.

with the increase in the value of λ, the third-order coefficient starts to provide an important contribution to the total coefficient. In fact, it shows a linear increment after

certain value of λ that is nearly the same value at which the linear and total optical absorption coefficients begin to show different behaviors.

A similar procedure of calculation, in this case for the relative change in the refractive index of the system, leads to the results shown in the Fig. 7. It can be seen that, in this case, the first and third order contributions have similar behaviors in regard of the variation of the peak amplitudes, as a consequence of the increment in the value of the inverse square potential parameter λ. As in Fig. 6(a), there is a non perceptible redshift in the curves. The first-order peak amplitude augments in the positive direction whilst the third-order peak amplitude diminishes (grows along the negative direction) [Fig. 7(a)]. The curves shown in the Fig. 7(b) confirm such features. One notices that the influence of augmenting the intensity of the inverse square potential reflects differently for the first- and third-order contributions of this quantity. The explanation for the variations exhibited by $\Delta^{(1)}/n$ and $\Delta^{(3)}/n$ follows the same arguments presented in the discussion of the results in Fig. 6. However, it is possible to observe that the third-order coefficient $\Delta^{(3)}/n$ is significantly
less sensitive to the variation of λ if compared with the first-order correction as well as with the corresponding dependence of the third-order optical absorption coefficient. We may see from Eqs. (18), (30), and (31) that $\Delta n/n$ is, in first-order, proportional to $\lambda^{1/2}$, whereas it becomes proportional to $\lambda^{3/2}$ in the case of the third-order contribution. Given that the values considered for the inverse square parameter are less than unity, this dependence explains the lowest rate of changing for the latter.

In addition, the Fig. 8(a) contains the results of the calculation for the total optical absorption coefficient as a function of the photon energy. In this figure, we have chosen to vary the intensity of the incident light and keep all the remaining parameters fixed. As we can see, the effect of augmenting the light intensity is apparent with regard to both the peak's height and symmetry. The height of the resonant peak is notoriously reduced if the incident light intensity increases. The particular features of the peak's asymmetry, which is practically unnoticeable for small intensities, now become more visible as long as the value of I grows. These facts can be explained by first noticing that the linear contribution to the optical absorption coefficient does not depend on the incident light intensity. Thus, its values remain unchanged if we modify the value of such input quantity. however, the third-order coefficient has a linear dependence with I which implies that as we increase the intensity, the magnitude of this coefficient grows, with – given the negative sign of this contribution – the consequent reduction of the total absorption peak height. It comes a moment when the value of the incident light intensity is so high that the total response at the frequency value of resonance turns to zero, as we may observe in the lowest curve of Fig. 8(a). Moreover, as the effect of increasing the intensity is more ap-

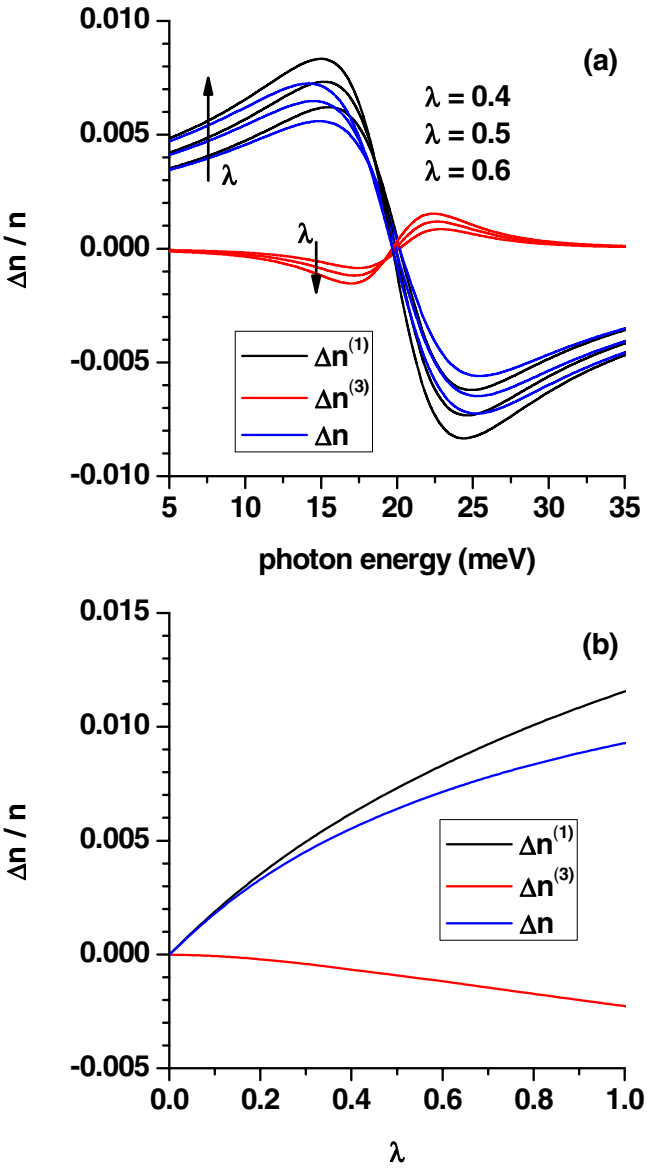

Figure 7 (online color at: www.ann-phys.org) Linear (black line), third-order nonlinear (red line) and total (blue line) relative refractive index change as a function of the photon energy (a) and the dimensionless parameter λ (b) with $\omega_0 = 1.2 \times 10^{13}\ \mathrm{s}^{-1}$, $B = 0$, and $I = 1.5 \times 10^{10}\ \mathrm{W/m}^2$ for Fig. (a). The direction of the arrows determines in which direction is raising λ for the the corresponding coefficients. In Fig. (b) we use the same parameters as well as $\hbar\omega = E_{21} - \hbar\Lambda_0$.

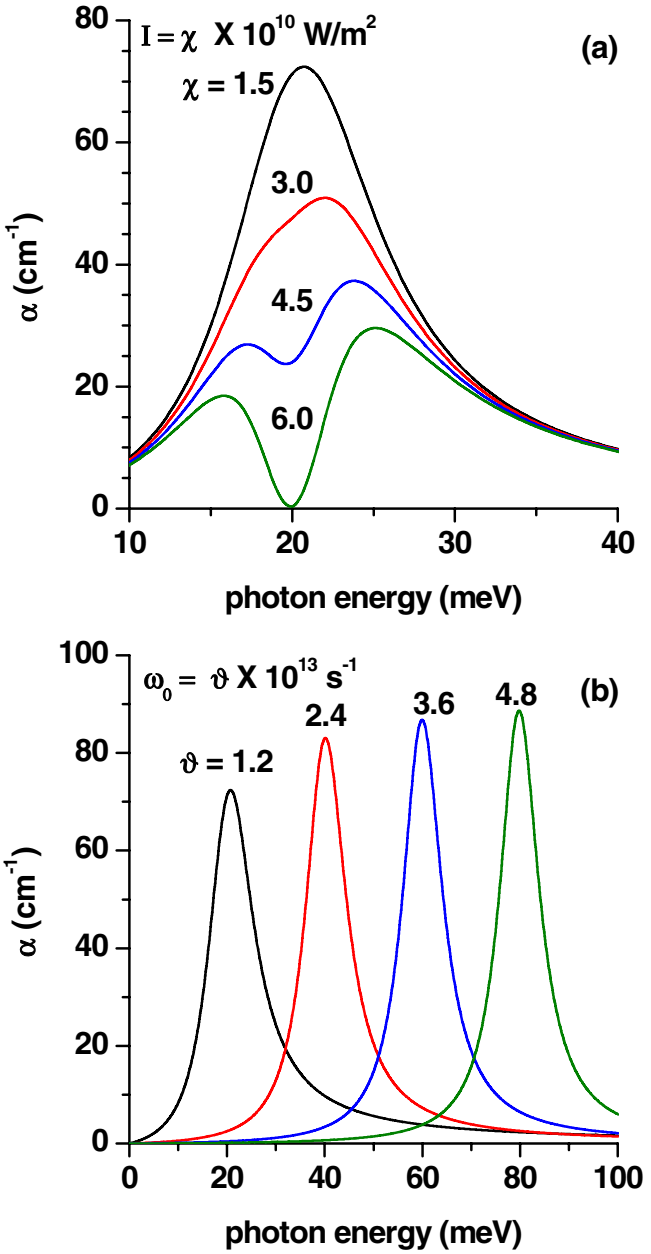

Figure 8 (online color at: www.ann-phys.org) Total optical absorption coefficient as a function of the photon energy. In both figures we use $\lambda = 0.5$, and $B = 0$. In Fig. (a) we use $\omega_0 = 1.2 \times 10^{13}\,\mathrm{s}^{-1}$ and vary the intensity I through a parameter χ as $I = \chi \times 10^{10}\,\mathrm{W/m}^2$. In Fig. (b) we use $I = 1.5 \times 10^{10}\,\mathrm{W/m}^2$ and vary ω_0 through a parameter ϑ as $\omega_0 = \vartheta \times 10^{13}\,\mathrm{s}^{-1}$.

parent, two different peaks begin to appear, in each case with different heights. This is a consequence of the dominant role played by the third-order coefficient, under such conditions.

In the Fig. 8(b) we are representing the curves for the total optical absorption coefficient, obtained by only varying the confinement frequency of the system, ω_0. It is possible to observe a blueshift in the resonant peak. Such an effect can be understood by looking at the expression for E_{21} given in the Eq. (18). The increase in ω_0 directly reflects in a raising of the energy difference. The second observed effect is the increasing of the peak intensity associated with the growth of the ω_0 value. This is mainly due to the fact that both the first- and third-order coefficients have a linear dependence on the energy of resonance, $\hbar\omega = E_{21}$, which is quantity that, as we already discussed, increases with the confinement potential energy. In this particular case, the electric dipole matrix element $|M_{21}|$ tends to decrease as a function of augmenting ω_0, leading us to conclude that, under the conditions present in the evaluation, the term proportional to the energy difference is the leading one, with dominance over the effect introduced by the term proportional to the electric dipole moment.

Under the same conditions taken into account to derive the results shown in the Fig. 8, we have obtained the corresponding variations of the relative change in the refractive index. They are presented in the Fig. 9. The influence of the variation in the incident light intensity appears in Fig. 9(a), which depicts the total $\Delta n/n$ as a function of the photon energy. In this case, one observes that augmenting the value of I results, in a progressive reduction in the resonant peak amplitudes. Once again, this can be explained by considering the increasing contribution coming from the third-order correction, which is the only one term depending on the light intensity – in a linear form. This term is always opposite in sign to the first-order one; thus its weight is progressively carrying importance into the total relative change. However, as we can see, the influence of this nonlinear term is – at least for the values of I considered here – not sufficient to invert the overall monotony of the quantity of interest, which is imposed by the dominance of the – intensity independent – linear contribution and $\Delta n/n$ keeps the same functional shape obtained for a fixed value of the incident intensity, and shown in Figs. 5 and 7.

The Fig. 9(b) presents the calculated relative change of the refractive index as a function of the incident photon energy with the variation of the degree of confinement posed by the parabolic potential term amplitude. We see now that, together with the blueshift of the resonant peaks, due to the direct dependence of the zero-correction frequency $\omega = E_{21}/\hbar$ on the value of the confinement frequency, ω_0. Nonetheless, the peak amplitudes are reduced by the influence of a higher degree of confinement because, in the case of this quantity,

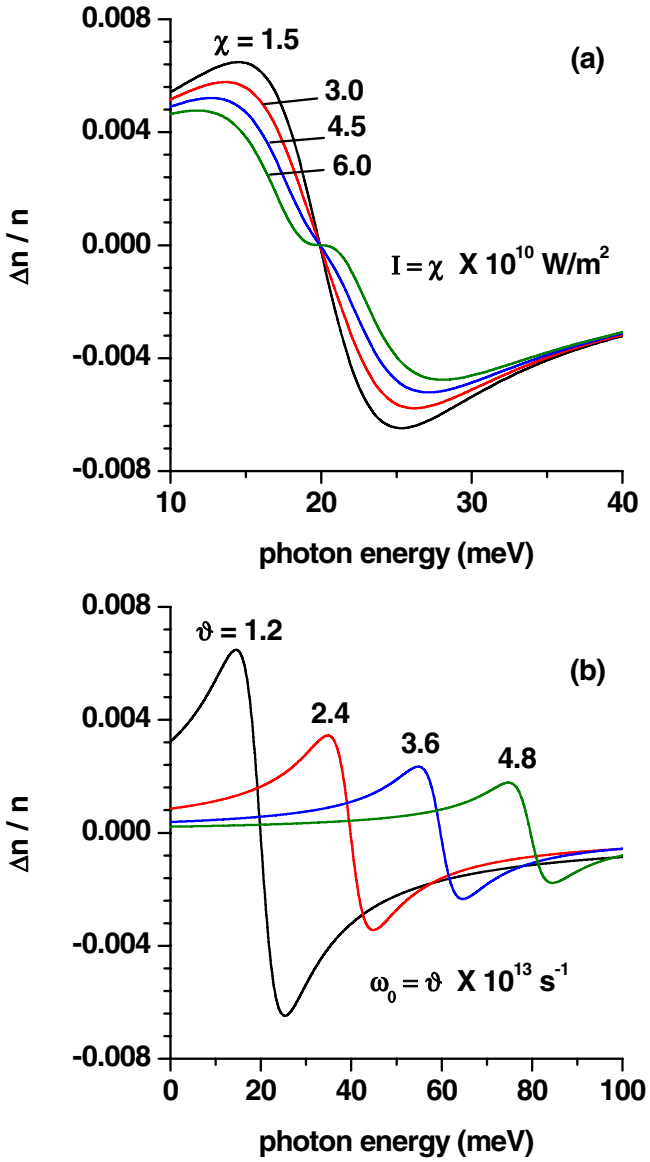

Figure 9 (online color at: www.ann-phys.org) Total relative refractive index change as a function of the photon energy. In both figures we use $\lambda = 0.5$, and $B = 0$. In Fig. (a) we use $\omega_0 = 1.2 \times 10^{13}\ \mathrm{s}^{-1}$ and vary the intensity I through a parameter χ as $I = \chi \times 10^{10}\ \mathrm{W/m}^2$. In Fig. (b) we use $I = 1.5 \times 10^{10}\ \mathrm{W/m}^2$ and vary ω_0 through a parameter ϑ as $\omega_0 = \vartheta \times 10^{13}\ \mathrm{s}^{-1}$.

the magnitude is dominated by the contribution of the dipole moment matrix element, which is an all the way decreasing function of ω_0.

4 Conclusions

In this article we have shown that the problem of finding the one-electron conduction states in a two-dimensional disc-shaped quantum dot with parabolic confinement, under the combined influence of an external magnetic field and an inverse square repulsive potential, has an exact analytical solution in the effective mass approximation. According to the symmetry of the obtained eigenstates, this particular potential energy configuration can be used to model the situation of parabolically confined quantum rings in 2D via a suitable choice of the involved parameters.

We have taken advantage of the states and energies so calculated to evaluate the intersubband linear and nonlinear contributions to the optical absorption coefficient as well as to the relative change in the index of refraction in the system under study. The results obtained reveal that the influence of the distinct input elements leads to different behaviors of these two quantities. In general, the augmenting values of both the magnetic field intensity and the parabolic confining amplitude have repercussions in the form of a blueshift of their resonant peaks. On the other hand, the increment in the amplitude of the inverse square potential reflects in an increment of the peak intensities for both coefficients. Finally, augmenting the intensity of the incident light, while remaining the other input elements with fixed values, makes the contribution coming from the third-order nonlinear terms to become more relevant, which causes an overall decrease in the resonant peak amplitudes in both the optical absorption and the refractive index relative variations.

The geometry of the system we have considered and the presence of the magnetic field perpendicular to the plane of the heterostructure makes this an excellent candidate for the calculation of other properties in the system such as: *i*) the presence of persistent currents and their dependence on geometry, which in this case by appropriate choice of the parameters of potential may be modulated from quantum disks to narrow quantum rings through wide quantum rings, *ii*) the absorption and photoluminescence spectra associated to magnetoexcitons, *iii*) the calculation of donor and acceptor properties for impurities confined in the heterostructure, and finally, *iv*) the effects of in-plane applied electric fields and hydrostatic pressure which can be used to amplify by several orders of magnitude the amplitude of the resonant peaks associated with the different nonlinear optical properties. Some of these works are currently under development and will be published elsewhere.

Acknowledgements. MEMR acknowledges support from Mexican CONACYT through grant CB-2008-101777. This research was partially supported by Colombian Agencies: COLCIENCIAS, CODI-Universidad de Antioquia (project: E01553-Propiedades ópticas no lineales en heteroestructuras semiconductoras de baja dimensionalidad (nitruros y arseniuros)), and Facultad de Ciencias Exactas y Naturales-Universidad de Antioquia (CAD-exclusive dedication project 2011-2012). The authors thank CONACYT (Mexico) and COLCIENCIAS (Colombia) for support under the 2012-2013 Bilateral Agreement "Estudio de propiedades ópticas, electrónicas y de transporte en sistemas de baja dimensión basados en carbono y semiconductores III-V: efectos de campos externos, temperatura y presión hidrostática". The work was developed with the help of CENAPAD-SP, Brazil.

Key words. Quantum dots and quantum discs, linear and nonlinear optical properties, parabolic confinement, inverse square potential, magnetic field.

References

[1] L. Brey, N. F. Johnson, and B. I. Halperin, Phys. Rev. B **40**, 10647 (1989).
[2] L. Brey, J. Dempsey, N. F. Johnson, and B. I. Halperin, Phys. Rev. B **42**, 1240 (1990).
[3] K. X. Guo and S. W. Gu, Phys. Rev. B **47**, 16322 (1993).
[4] X. Hong Qi, X. Jun Jong, and J. J. Li, Phys. Rev. B **58**, 10578 (1998).
[5] L. Zhang and H. J. Xie, Phys. Rev. B **68**, 235315 (2003).
[6] L. Zhang, Superlatt. Microstruct. **37**, 261 (2003).
[7] C. Zhang and K. X. Guo, Physica B **383**, 183 (2006).
[8] P. M. Petroff, A. Lorker, and A. Imamoglu, Phys. Today **54**, 46 (2001).
[9] D. Bimberg, M. Grundman, and N. N. Ledentsov, Quantum Dot Heterostructures (John Wiley Sons, Chichester, 1999).
[10] O. Benson, C. Santori, M. Pelton, and Y. Yamamoto, Phys Rev Lett. **84**, 2513 (2000).
[11] F. Suárez, D. Granados, M. L. Dotor, and M. G. García, Nanotechnology **15**, S126 (2004).
[12] H. S. Ling, S. Y. Wang, C. P. Lee, and M. C. Lo, J. Appl. Phys. **105**, 034504-1 (2009).
[13] F. Troiani, U. Hohenester, and E. Molinari, Phys. Rev. B **62**, R2263 (2000).
[14] W. E. Kerr, A. Pancholi, and V. G. Stoleru, Physica E **35**, 139 (2006).
[15] B. Tatievski, P. Stampfli, and K. H. Bennemann, Ann. Phys. (Berlin) **4**, 202 (1995).
[16] W.-C. Tan and J. C. Inkson, Phys. Rev. B **60**, 5626 (1999).
[17] Y. Avishai and M. Kohmoto, Phys. Rev. Lett. **71**, 279 (1993).
[18] G. H. Wang and K. X. Guo, Physica B **315**, 234 (2002).
[19] G. H. Wang and K. X. Guo, Physica E **28**, 14 (2005).
[20] C. H. Liu, K. X. Guo, C. Y. Chen, and B. K. Ma, Physica E **15**, 217 (2002).
[21] W. F. Xie and Q. Xie, Physica B **404**, 1625 (2009).
[22] S. J. Liang and W. F. Xie, Physica B **406**, 2224 (2011).
[23] N. F. Johnson and L. Quiroga, Phys. Rev. Lett. **74**, 4277 (1995).
[24] D. Ahn and S. L. Chuang, IEEE J. Quantum Electron. **QE23**, 2196 (1987).
[25] E. E. Kummer, J. Reine Angew. Math. **17**, 228 (1837).